

Self-Supervised Representation Learning for Detection of ACL Tear Injury in Knee MRI

Siladitya Manna

CVPRU, Indian Statistical Institute

Kolkata, India

siladitya_r@isical.ac.in

Saumik Bhattacharya

E&ECE, Indian Institute of Technology

Kharagpur, India

saumik@ece.iitkgp.ac.in

Umapada Pal

CVPRU, Indian Statistical Institute

Kolkata, India

umapada@isical.ac.in

Abstract—The success and efficiency of Deep Learning based models for computer vision applications require large scale human annotated data which are often expensive to generate. Self-supervised learning, a subset of unsupervised learning, handles this problem by learning meaningful features from unlabeled image or video data. In this paper, we propose a self-supervised learning approach to learn transferable features from MRI clips by enforcing the model to learn anatomical features. The pretext task models are designed to predict the correct ordering of the jumbled image patches that the MRI frames are divided into. To the best of our knowledge, none of the supervised learning models performing injury classification task from MRI frames, provide any explanations for the decisions made by the models, making our work the first of its kind on MRI data. Experiments on the Pretext task show that this proposed approach enables the model to learn spatial context invariant features which helps in reliable and explainable performance in downstream tasks like classification of ACL tear injury from knee MRI. The efficiency of the novel Convolutional Neural Network proposed in this paper is reflected in the experimental results obtained in the downstream task.

Index Terms—Self-supervised, representation learning, MRI

I. INTRODUCTION

Deep Learning techniques have displayed great success in computer vision tasks like object detection, tracking or segmentation. These deep learning models are trained on large datasets containing millions of samples or several gigabytes of human annotated data. Hence, these techniques fall under the paradigm of Supervised Learning. The models that are trained on large datasets can again be used as pre-trained network to get faster convergence in several tasks, because they already have learnt hierarchical features and greatly reduce the overfitting problem. However, annotating such huge amount of data is really time consuming and requires human labor, thus making it somewhat expensive to collect. In many cases, especially for medical data, specific expertise is needed to perform the annotation task which is often difficult to find. Because of the cost and labor associated with supervised learning, several attempts have been made to come up with techniques which can help the machine learning models learn good representation of the underlying data distribution without the availability of large amount of annotated data. Recent advances made in this regard, includes Transfer Learning, semi-supervised learning, weakly-supervised learning, domain adaptation and unsupervised learning strategies [28]–[31]

In this paper, we have concentrated our efforts on self-supervised representation learning, which falls under the canopy of unsupervised learning. The main objective of self-supervised learning is to learn good feature representations from large-scale spatial or temporal visual data without the help of human supervision. This objective is generally achieved by solving pretext tasks. Several *pretext* tasks have been proposed for self-supervised representation learning and these include image inpainting [21], solving jigsaw puzzles [4], [10], temporal order correction [3], [5], [24], geometric transformation prediction [3], [7], [20], [21], etc. To solve these pretext tasks, the required self-supervision comes by means of devising *pseudo-labels* which serve as the ground truth. The pretext tasks and the associated pseudo-labels are generally defined depending on the nature of the data. The objective of the pretext task is to extract explainable and transferable representations that can be useful in solving a *downstream* tasks, such as, object detection, tracking, semantic segmentation etc.

Several approaches of self-supervised learning strategies include designing pretext tasks in which the objective is to predict the geometric transformations applied on the images or videos [3], [7], [20], [21]. Learning rich visual representations from videos have also been achieved by designing pretext tasks which predicts the temporal order of the permuted frames from videos [3], [5], [24]. Generative models based approaches like image inpainting [21], predicting future frames in video [17], image colorization [23] also helps in learning higher-level visual representation from the data. Other spatial structure based pretext tasks are also designed for different natural image classes [4], [10], [25]. However, in medical image analysis, application of self-supervised learning methods is limited. Jiao et al. (2018) [3] applied a combination of temporal order correction and geometric transformation prediction methods for standard plane detection in fetal ultrasound videos.

The main objective of our paper is to propose a self-supervised representation learning method to learn features from knee MRI without human annotations. These features will then be used to reliably detect injuries sustained in the knee of a human. The pretext task in our method follows the Jigsaw Puzzle solving strategy of learning visual representations. We have shown with rigorous experimental evidences that this method helps the self-trained models to learn spatial

context invariant features in MRI clips. The downstream task in our paper is to classify ACL tear injury in the Knee MRIs using the features learnt by the pretext model.

Our contributions in the work are as follow.

- We propose a novel Convolutional Neural Network architecture for Jigsaw Puzzle solving as pretext task. This model can be trained from scratch to learn explainable visual representational features.
- We also propose an unique *Divide-and-Teach* strategy to train the model for the Downstream task in case of GPU memory constraint. This strategy also enables the model to learn temporally independent features.
- To the best of our knowledge, this work is the first of its kind in Self-supervised representation learning domain targeted for Knee MR videos.
- Our work is demonstrated to be effective in extracting explainable and transferable context invariant features, evident from results obtained in the Downstream tasks.

II. METHODS

Our goal is to learn feature representation of the spatial and temporal information that is available from the Magnetic Resonance videos. We achieve this goal by devising a novel CNN architecture, which predicts the order in which the patches have been jumbled or rearranged. In the following subsections, we focus on designing the pretext algorithm and subsequently the Downstream algorithm for detecting ACL tear injury from knee magnetic resonance videos.

A. Pretext Task Algorithm

The pretext task in our method is similar to Jigsaw Puzzle solving strategy. However, it can also be described to be more similar to solving a sliding puzzle or more preferably Jumbled Patch Order Prediction strategy. In this learning strategy, we divide a randomly chosen frame from a MRI clip into N square patches of dimension $\lfloor \frac{L}{\sqrt{N}} \rfloor \times \lfloor \frac{L}{\sqrt{N}} \rfloor$, where L is the dimension of the square frame, N is the number of patches we want to divide the frame into, and $\lfloor x \rfloor$ equals the nearest integer less than or equal to x . Dividing the frame into N patches gives $N!$ ways to jumble the patches. For $N = 9$, we have $9! = 3,62,880$ rearrangements. Let us denote the set of all the rearrangements as \mathcal{J} . Also, let the rearrangement, applying which the frame remains ordered, as in Fig. 1, be denoted by τ_0 .

Since solving a classification task with such a large number of classes would require a huge amount of data and computational time, we choose a subset \mathcal{A} of the set \mathcal{J} by following the Algorithm 1 which describes the steps we use to choose the permuted rearrangement orders to be included in \mathcal{A} . We initialize the set of arrangements with the ordered arrangement $[1, 2, 3, 4, 5, 6, 7, 8, 9](\tau_0)$ and choose the threshold of hamming distance as $\lfloor \frac{N}{2} \rfloor$. The hamming distance between two permutations is defined as the number of positions in which they differ. In our experiments, we consider $N = 9$, thus the threshold of hamming distance equates to 4. We progressively keep on adding elements from the set \mathcal{J} if its

Algorithm 1: SETARR : How to choose the set of arrangements

Result: \mathcal{A} : Set of Arrangements

Initialize $\mathcal{A}' = \{\tau_0\}$;

Given \mathcal{J} : Set of all possible arrangements

for $i = 1:9!$ **do**

$d = 0$

for a in \mathcal{A}' **do**

$d = d + \text{hammingDist}(a, J[i])$

end

$d = \frac{d}{|\mathcal{A}'|}$

if $d \geq 4$ **then**

$\mathcal{A}' = \mathcal{A}' \cup \{J[i]\}$;

end

end

$\mathcal{A} \sim \mathcal{U}[\mathcal{A}']$

average hamming distance from the elements in the set \mathcal{A}' is more than or equal to 4. This algorithm ensures that the elements in the chosen set do not lie in a crowded region in the permutation space. Otherwise it becomes too difficult for the model to differentiate between them. It also ensures that the elements are not too far away from each other or the task will become too easy for the model.

Running the above algorithm on \mathcal{J} resulted in a subset of about 12K permutations. But this number is still too high to train a CNN model in reasonable amount of time and with limited computational resources. Hence, we adopted a uniform random sampling without replacement strategy, where the samples are drawn from an uniform distribution to choose $|\mathcal{A}|$ arrangements from the chosen 12K arrangements. In Algorithm 1, $\mathcal{U}[\mathcal{A}']$ denotes uniform random sampling on the set \mathcal{A}' . It should be noted that the number of arrangements $|\mathcal{A}|$ is equal to the number of classes \mathcal{C} in the pretext classification task.

To prevent the network from learning both inter-patch low level signals like discontinuities in pixels patterns and intra-patch low level signals like edges, corners and black pixel regions, we applied data augmentations to each rearranged patch. This also helps in making the model robust. We choose the geometric transformation to be applied from a finite set \mathcal{G} , which can be expressed as a Cartesian product of four finite sets \mathcal{R} , \mathcal{T}_x , \mathcal{T}_y and \mathcal{S} , i.e., $\mathcal{G} = \mathcal{R} \times \mathcal{T}_x \times \mathcal{T}_y \times \mathcal{S}$ where $\mathcal{R} = \{-15, 0, 15\}$, $\mathcal{T}_x = \{-[0.1L_p], 0, [0.1L_p]\}$, $\mathcal{T}_y = \{-[0.1L_p], 0, [0.1L_p]\}$ and $\mathcal{S} = \{1, 1.2\}$. Here \mathcal{R} , \mathcal{T}_x , \mathcal{T}_y , \mathcal{S} denote the finite sets of angles of rotation in degrees, magnitude of translation along x -axis and y -axis in pixels and scale factors, respectively. L_p denotes the dimension of each side of a square patch. This gives us 54 combinations of geometric transformations, all to be chosen randomly. In addition to the geometrical transformation, we also apply Gamma correction with γ values chosen from the finite set $\{0.85, 1.00, 1.15\}$. The purpose behind applying Gamma correction is to ensure that the model learns structural features from the MRI clips instead

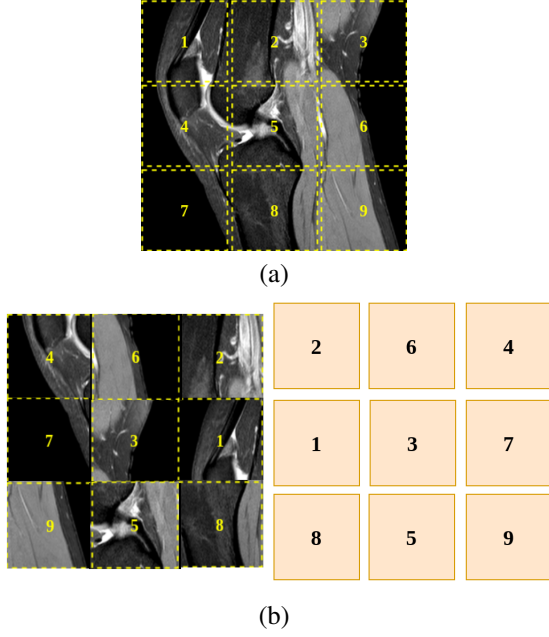


Fig. 1. Input patch ordering. (a) Image showing the numbering of the patches in an ordered frame. (b) Image showing the numbering of the patches in a jumbled frame and the corresponding channels the patches are fed into (output node is in the direction of looking into the page perpendicularly).

of features based on pixel intensities.

It should be mentioned here that $L_p \neq \frac{L}{\sqrt{N}}$. Every patch is obtained by randomly cropping a 64×64 patch out of the $\lfloor \frac{L}{\sqrt{N}} \rfloor \times \lfloor \frac{L}{\sqrt{N}} \rfloor$ patch. In our experiments, $\lfloor \frac{L}{\sqrt{N}} \rfloor = 85$. So, we have a 21 pixels buffer region in each patch by which the 64×64 patch can be randomly shifted to obtain different patches. By doing this, we ensure a minimum gap of 0 pixel and a maximum of 42 pixels gap between two neighbouring patches. These 64×64 patches are then fed to the network as input after rearrangement.

To obtain the Jumbled Patches (Fig. 2) and the Pseudo-labels, we apply Algorithm 2 to the frames randomly sampled from each MRI sample. Geometric transformation g is obtained by uniformly sampling an element from the set of geometric transformations \mathcal{G} and applied to each patch. 64×64 patch is obtained by first uniformly sampling values for the reference points $(refx, refy)$ from the range $[0, \lfloor \frac{L}{\sqrt{N}} \rfloor - 64]$, and then cropping a 64×64 patch from the larger patch with the reference point $(refx, refy)$ as its origin.

The random pseudo-label selection process and random augmentations applied to each patch, forces the network not to learn features which spatially correlates two neighbouring patches. Instead, it forces the network to learn spatial context invariant feature representations.

B. Issues with Pretext Tasks

The primary issue that occurs when training a *pretext* task is that the pretext task models are very prone to learning low level signals. When using the Jigsaw Puzzle solving strategy without the augmentations, the model tends to learn low level signals similar to the clues that humans often use when solving

Algorithm 2: PREPFRAM : How to prepare each frame for training

Result: \mathcal{P}_A : Jumbled Patches from a frame \mathcal{F}

Initialize

\mathcal{F} = a random frame from a MRI sample

$\mathcal{P}_A = \{\}$

$\mathcal{L}' = \lfloor \frac{L}{\sqrt{N}} \rfloor$

$row = col = refx = refy = 0$

Given

A : Set of rearrangements

\mathcal{G} : Set of geometric transformations

Sample $\tau = \mathcal{U}[A]$

for $i=1:9$ **do**

$row = \lfloor \frac{i}{\sqrt{N}} \rfloor$

$col = i \bmod \sqrt{N}$

$\mathcal{P}' = \mathcal{F}[row.\mathcal{L}' : (row + 1)\mathcal{L}', col.\mathcal{L}' : (col + 1)\mathcal{L}']$

$g = \mathcal{U}[\mathcal{G}]$

$\mathcal{P}' = g(\mathcal{P}')$

$refx = \mathcal{U}[0, \mathcal{L}' - 64]$

$refy = \mathcal{U}[0, \mathcal{L}' - 64]$

$\mathcal{P}' = \mathcal{P}'[refx : refx + 64, refy : refy + 64]$

$\mathcal{P}_A = \mathcal{P}_A \cup \mathcal{P}'$

end

Jigsaw Puzzles. The approach we follow in this paper also compels us to take a subset of the large pool of possible rearrangements. Otherwise the required computational time would become huge. To choose the permutations we follow an approach similar to the one followed in [4] with necessary changes.

As MRNet dataset contains grayscale data, the presence of black pixels in the images is a lot more than in natural images. The dataset contains 1130 training samples, but the difference in content or information between the frames of two different clips at almost the same time step is very little. Thus, the variation in information over the whole training set is not large. This makes it difficult for the model to differentiate between two almost identical samples.

In one of our initial models we used a single Inception-ResNet-v2 network pre-trained on ImageNet, to detect the arrangements. The input was all the 9 patches put together like in Fig. 2. The model used the low level signals like patterns of black pixels, corners, edges and discontinuities between patches to learn discriminative features. This is shown in the gradient class activation mappings [2] in Fig. 3. This tendency of the model to learn shortcuts to the global minima of the loss surface prevents it from learning context invariant visual representational features. Fig. 3 shows the gradcam [2] outputs of the aforementioned model along with the ground truth label and the probability of prediction.

C. Pretext Task Model Architecture

In our paper, we have used a semi-parallel architecture for our pretext tasks. The final network model architecture used

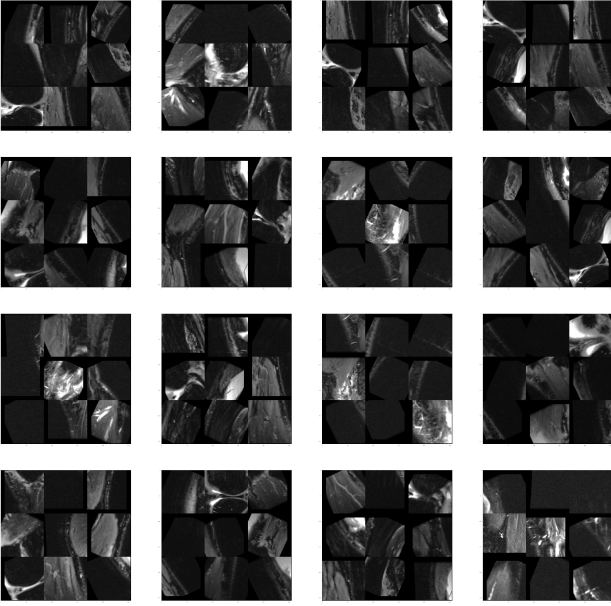


Fig. 2. A single batch of jumbled frames

for the pretext tasks in our experiments is shown in Fig. 4. As we divided the input image into 9 patches, we feed each of the 9 patches into one of the 9 parallel Convolutional channels. Each convolutional channels is made up of 2 Convolutional blocks. Each convolutional block consists of two convolutional layers followed by a Max Pooling layer. The number of filters of both the convolutional layers, in the two convolutional blocks are 256 and 512, respectively. The Max Pooling layer has a pool window of size 2×2 and stride 2.

The output from all the 9 channels are then concatenated to get a output volume of shape $8 \times 8 \times 4608$. This output volume is then convoluted with 1×1 filters to reduce the dimensionality and gives an output of shape $8 \times 8 \times 1024$ which is then fed into two channels. The first channel is a convolutional block, which consists of two convolutional layers with 1024 filters, with the second layer having stride 2, thereby causing the resolution of the output to be reduced to half of the input. The second channel contains a convolution layer with 1024 filters with kernel size 1×1 and followed by a max pooling layer which reduces the dimensions to half. The reason for using this second 1×1 layer is simply to increase the non-linearity of the model. The outputs from the two channels are again concatenated to form an output volume of $4 \times 4 \times 2048$. Global average Pooling is applied to this output volume of shape $4 \times 4 \times 2048$ to obtain an output of shape 2048, which is then fed into a fully connected layer of length 1024, followed by another Fully Connected layer of the same length. The second Fully Connected layer is connected to the output consisting of \mathcal{C} nodes, where \mathcal{C} is the number of classes.

During the Downstream task, only the convolutional layers from the 9 channels are used. So the quality of the features learnt in the pretext task play an important role in the down-

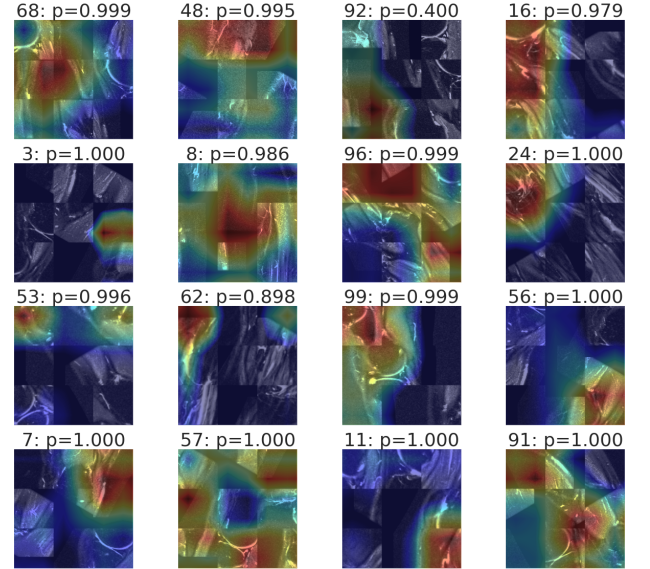


Fig. 3. Gradcam output shows the regions (indicated by red) where the model built using pre-trained Inception-ResNet-v2 gains maximum information from. It is clearly visible that the maximum attention is on the low level signals as mentioned in Section II.B

stream tasks.

D. Downstream Task Algorithm

In this paper, the objective of the downstream task is to predict whether the knee has sustained injury to the Anterior Cruciate Ligament or not.

Algorithm 3: DIVFRAM : How to divide the frames

Result: \mathbf{I} : List of Inputs

Initialize

$\mathbf{I} = []$;

start_index = 0;

end_index = 0;

Given

\mathbf{F} : All frames in the MRI clip

\mathbf{N} : Number of frames

for $i = 1:\mathbf{N}$ **do**

$n = \lceil \frac{\mathbf{N}}{9-i+1} \rceil$

end_index = **end_index** + n

Append $\mathbf{F}[\text{start_index} : \text{end_index}]$ to \mathbf{I}

start_index = **end_index**

end

For performing the downstream task, we construct a model (Fig. 5) consisting of two parts, *feature extractor* and *discriminator*. The model, self-trained using the pretext tasks acts as the feature extractors. The feature extractor part consists of the 9 convolutional channels from the pretext task model.

In our paper, we devise an unique *Divide-and-Teach* training methodology. As we have seen that the pretext task consists of 9 channels through which different patches have been at different points of time during the training process. So, it is

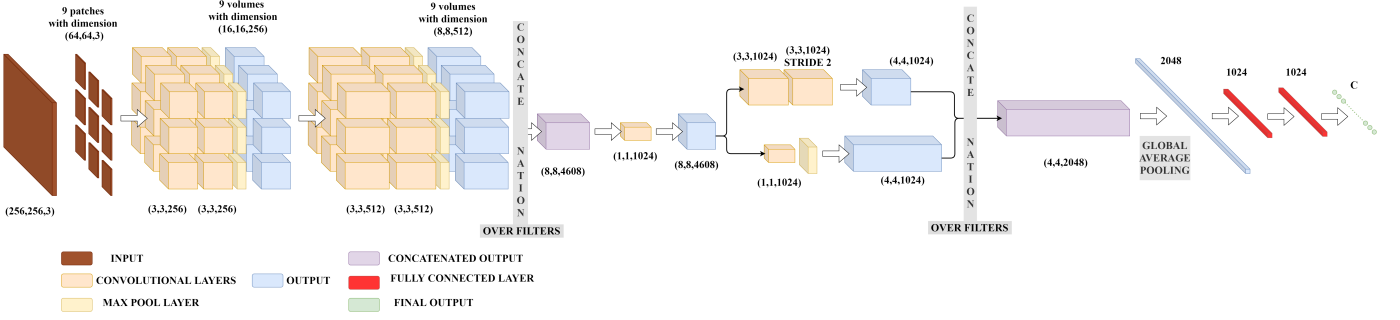


Fig. 4. Network model for Pretext Task

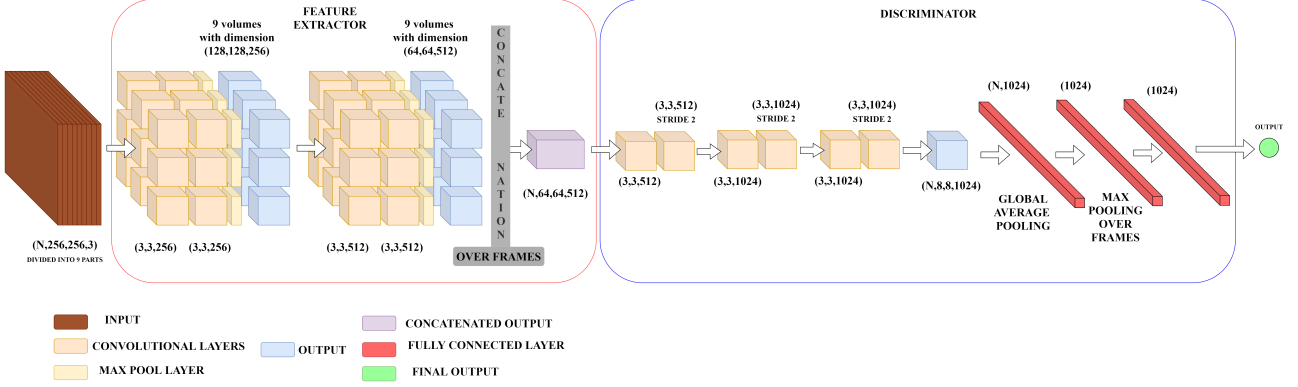


Fig. 5. Network model for Downstream Task

expected that convolutional layers of the respective convolutional blocks in all the channels will learn features which are context invariant and more or less similar. That being said, we can safely claim that each convolutional layer is capable of extracting useful features from the frames, irrespective of the temporal position of the frame in the MRI clip. We divide $|F|$ frames into 9 parts before feeding to the 9 channels of the CNN, $|F|$ being the total number of frames in the MRI sample. After the respective outputs are obtained from each channel, we concatenate the outputs over the frames to obtain an output of shape $|F| \times 64 \times 64 \times 512$. These features are then fed into the discriminator.

The Discriminator consists of three convolutional blocks, each containing two convolutional layers. Both the layers in each convolutional block has filter size 3×3 but only the second convolutional layer has stride 2. This reduces the dimensions to half without the use of Max Pooling layers. The three convolutional layers result in an output of shape $|F| \times 8 \times 8 \times 1024$. We then apply Global Average Pooling to the output, followed by max pooling over frames [1]. This gives an output of length 1024, which is then fed into a network of two fully connected layers, each containing 1024 nodes. The output from this layer is finally fed into the output node. The downstream task is a binary classification task, hence sigmoid activation is applied on the output node to obtain predictions in the 0 to 1 range.

To prevent the self-trained CNN layers from learning

temporal-specific features during the fine-tuning process, we shuffle the list of inputs \mathbf{I} , such that the frames at i^{th} position are not fed into the i^{th} channel. Concatenating the outputs from the 9 convolutional channels of the Feature Extractor, we get back an output of shape $|F| \times 64 \times 64 \times 512$ but this output is not ordered temporally. The Discriminator takes these extracted features as input, with one input arranged in a different temporal order than the previous one. Shuffling the temporal order of the frames helps the model in learning mode generalized features. This strategy also helps the model in dealing with missing frames and sparse temporal data. The gradient class activation mappings [2] are presented in section III. D.

Apart from the above *Divide-and-Teach* training strategy, data augmentations like random rotation, translation and scaling were also applied on each frame during training. The augmentations applied were different for different elements of the input \mathbf{I} . In addition to the above augmentations we also added *Gaussian Noise* to the frames from the training set samples to make the model more robust and reduce generalization error.

III. EXPERIMENT AND RESULTS

A. Dataset

In our experiments, we use the MRNet [1] dataset as our reference dataset. The MRNet dataset [1] contains 1370 knee MRI clips in total. Out of 1370 clips, 1130 MRI clips are

included in the training set and 120 MRI clips are considered as the tuning or validation set. The rest 120 are used for external validation and is hidden. The classes in the dataset are Abnormality, ACL Tear and Meniscus Tear. Out of the 1,130 training examples, 917 are Abnormal exams, 208 are ACL tears and 397 examples are Meniscus tears. The MRNet Dataset is a multi-label dataset and is imbalanced in nature. This gives us an opportunity to explore the effects of self-supervised learning techniques on imbalanced datasets.

B. Pretext Task Experimental Details

During training, the model was trained with frames chosen following the strategy discussed in Section II.B. We optimized the Categorical Crossentropy loss of the model using Adam optimizer with a small learning rate of 10^{-4} . We used a batch size of 32 during both training and validation stages. However, during the validation stage, we used neither data augmentation on the patches nor gamma correction on the frames, because our ultimate goal is to extract features from frames which are not jumbled. Hence, it seemed logical to tune the network only on the ordered frames. No augmentation was applied on the frames as a whole. The pretext model was trained entirely from scratch on a NVIDIA RTX 2080Ti 11GB GPU. The training was stopped when the Validation accuracy showed signs of flattening.

C. Pretext Task Results

Intuitively, the main objective of the pretext task should be to learn features which will contribute more towards the downstream task. In our paper, we have presented the results pertaining to detection of ACL tear injury in Knee MRI. In the Fig. 6 we can see the Region of Interest which needs to be focused on primarily to get good performance on the downstream task. From the gradient class activation mappings [2], as shown in Fig. 7, we see that the pretext task model has reliably focused on the important structural parts of knee where the Anterior Cruciate Ligament exists. Thus, it provides explainability to the downstream task which is absent in most of the recent deep models. To further analyze the capacity of the model, we select 1000 random permutations as mentioned in Algorithm 1 and train the model by changing the final layer accordingly. As shown in Table 1, even after increasing the number of permutations, the proposed model performs well and finds out the relevant structures from the MRI frames.

TABLE I
PRETEXT TASK EXPERIMENTAL RESULTS

Arrangements	Training Accuracy	Validation Accuracy
500	87.3%	85.4%
1000	71.7%	68.5%

D. Downstream Task Experimental Details

In the downstream task, due to memory constraint on the NVIDIA RTX 2080Ti, we limited the number of frames to

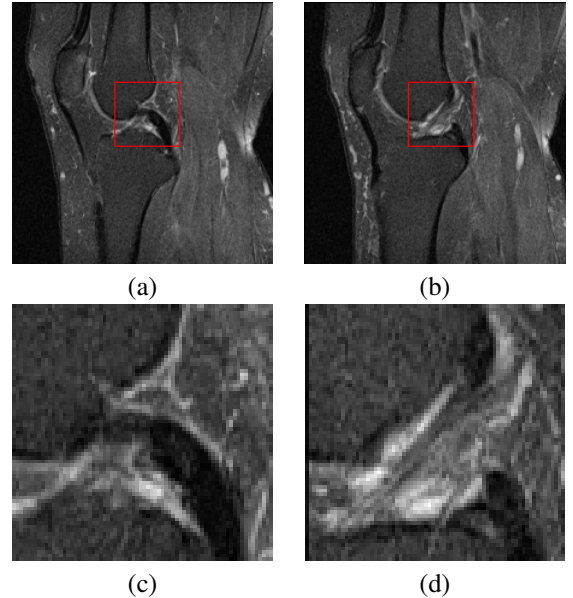


Fig. 6. Region of Interest for ACL tear Detection. Image (c) and (d) showing the enlarged view of the ROIs marked in red in the image (a) and (b), respectively.

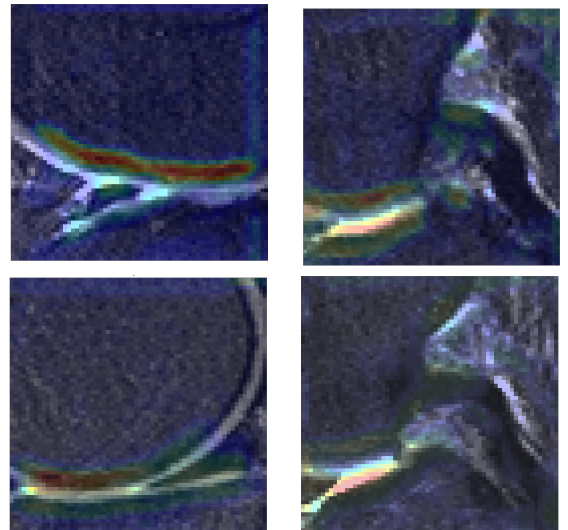


Fig. 7. Gradient Activation Class Mappings on the 64×64 patches showing the attention the pretext task model gives on the Anterior Cruciate Ligament

$\min(|F|, 27)$, where $|F|$ is the number of frames in the MRI clips. If the number of frames in any MRI clip is more than 27, we use uniform random sampling to select 27 frames from $|F|$ number of frames. This strategy helps the model deal with missing frames and sparse temporal data. Also, we kept the batch size limited to 1. We optimized the binary crossentropy loss of the model using Adam Optimizer with an initial learning rate of 10^{-5} . Since the dataset is highly imbalanced, we used oversampling to balance the dataset before training our model. The number of positive ACL tear injury samples in the MRNet Dataset is 208 and the number of negative samples is 922. To do away with this imbalance,

TABLE II
DOWNSTREAM TASK RESULTS FOR MODELS OF DIFFERENT CAPACITIES

Model	Number of Parameter	Accuracy (95% CI)	AUC (95% CI)
Proposed	77 Million	76.62 (74.5,78.83)	0.8481(0.8284,0.8651)
Model-2	75 Million	73.4 (71.0,75.6)	0.834 (0.812,0.850)
Model-1	72 Million	71.7 (70.2,72.9)	0.813 (0.797,0.829)

we over-sampled the minority class (positive) to 922. This over-sampled dataset was then used to train the downstream model. During the Validation stage, we did not apply random shuffling of the frames or any type of data augmentation, but we chose $\min(|F|, 27)$ number of frames and then partitioned the frames into 9 parts.

E. Downstream Task Results

In the downstream task, we gradually increased the number of parameters by adding different layers. As the number of parameters is increased, the models' capability of approximating the function from the input space to the output space increases. It can be observed from the results presented in Table II that increasing the number of parameters boosts the performance, even when the positive samples are under-represented during the pretext task. For the ACL tear detection task, the best results were obtained using our final model with 77 Million parameters. It achieved an accuracy of 76.62% (95% CI 74.50, 78.83) on the Validation set and an AUC score of 0.8481 (95% CI 0.8284, 0.8651).

From the gradient class activation mappings [2] in Fig. 8, it can be seen that the downstream model also focuses on the desired region, required for it to detect the ACL tears. Though, there are some models that perform the classification task of injury from MRI frames, to the best of our knowledge, none of them provides any insight or explanation for the decision made by their models. Thus, we could not compare the performance of our model with any existing method.

F. Ablation Studies

To optimize our model architecture, we built multiple models by changing the different hyperparameters associated with the model. Among all the variants, the model shown in Fig. 5 corresponds to the final model which performed the best in the downstream task. In a variant model (Model-1), a Max Pooling layer was introduced instead of the first convolutional block in the Discriminator and the two convolutional layers in the second convolutional block contained 512 filters each. Also only one Fully Connected layer was used in Model-1. In the second variation (Model-2), we increased the capacity by adding another fully connected layer with 1024 nodes and increasing the number of filters of the convolutional layers in the second convolutional block to 1024. The Max Pooling layer in the Discriminator of Model-1 remain unchanged in Model-2. In the best performing model (Model-3), we replaced the Max Pooling layer in the discriminator by a convolutional

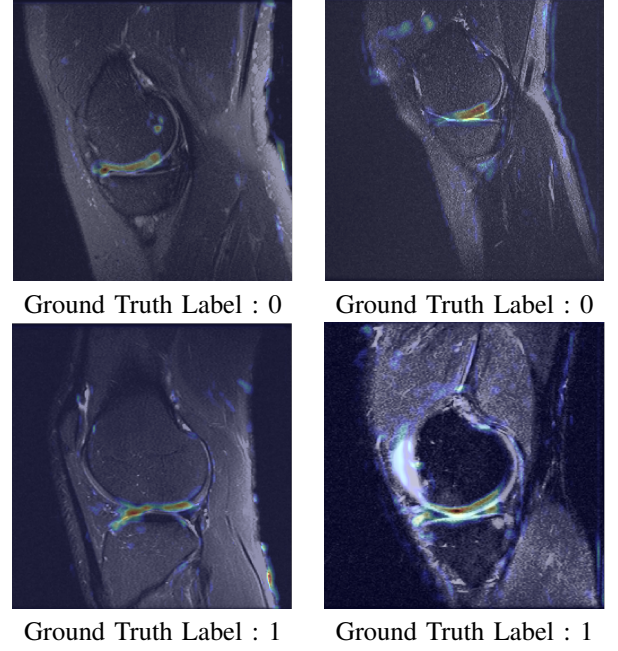


Fig. 8. Gradient Activation Class Mappings on the 256×256 frames shows that the downstream task model focuses on the Anterior Cruciate Ligament

block, containing two convolutional layers, each with 512 filters. The performance results of all the three models have been shown in Table II. We observed that further addition of convolution layer increased the model complexity without any effective change in performance.

G. Effects of Class Imbalance

The pretext task and the downstream task, both contributes to the ultimate objective of detection of ACL injury from knee MRI. The motivation of our work is to build a pretext model, capable of learning spatial context invariant visual representational features. In our experiments, 0 represents the majority class and 1 represents the minority class. The results presented in Table III show that in case of an imbalanced dataset, the features of the majority class receive more weightage than the minority class in the pretext task and hence were learnt better, even though the pretext models are trained using pseudo-labels. Every sample in the training set is chosen exactly once when preparing the pseudo training samples in the pretext task. Thus for each pseudo-label, there are more samples from the majority class than from the minority class.

When the oversampled dataset is used to train the model in the pretext task, equal number of samples from both classes are selected for preparing the pseudo training samples. Thus, the features from both the original classes are learnt with equal weightage. The pretext model achieved Training and Validation accuracy of 91.2% and 90.6% respectively. The downstream model showed an increase in the *True Positive Rate* and a reduction in *Type 2 error*. However, *Type 1 error* increased slightly, subsequently lowering *True Negative Rate*.

TABLE III
ABLATION STUDY ON THE TASK OF DETECTION OF ACL TEAR INJURY

Model	Accuracy (95% CI)	AUC (95% CI)	Sensitivity (95% CI)	Specificity (95% CI)
without oversampling	76.62% (74.5,78.63)	0.8481 (0.8284,0.8651)	0.5908 (0.5511,0.6223)	0.9062 (0.8799,0.9275)
with oversampling	76.72% (74.90,78.70)	0.8479 (0.8264,0.8701)	0.7395 (0.7132,0.7757)	0.7881 (0.7599,0.8182)

IV. CONCLUSION

The objective of this work is to explore the possibilities that Self-supervised learning provides in Deep Learning applications, particularly in medical image analysis domain. It has been shown that our proposed pretext model extract structural features particularly from the region of interest which can support a downstream task of classification further. The challenges associated with this pretext task are discussed and analyzed thoroughly. However, approaches involving self-supervision depend largely on the quality of the features that the pretext models learn and this shapes the performance of the downstream task. We look to further explore other techniques which can accommodate different kinds of injuries in a single downstream task by learning more robust and meaningful visual representational features in the pretext tasks.

REFERENCES

- [1] Bien, N., Rajpurkar, P., Ball, R.L., Irvin, J., Park, A., Jones, E., Bereket, M., Patel, B.N., Yeom, K.W., Shpanskaya, K.S., Halabi, S.S., Zucker, E.J., Fanton, G.S., Amanatullah, D.F., Beaulieu, C.F., Riley, G.M., Stewart, R.J., Blankenberg, F., Larson, D.B., Jones, R., Langlotz, C.P., Ng, A.Y., & Lungren, M.P. (2018). Deep-learning-assisted diagnosis for knee magnetic resonance imaging: Development and retrospective validation of MRNet. *PLoS Medicine*, 15. Phil. Trans. Roy. Soc. London, vol. A247, pp. 529–551, April 1955.
- [2] Selvaraju, R.R., Cogswell, M., Das, A., Vedantam, R., Parikh, D., & Batra, D. (2017). Grad-CAM: Visual Explanations from Deep Networks via Gradient-Based Localization. 2017 IEEE International Conference on Computer Vision (ICCV), 618-626.
- [3] Jiao, J., Droste, R., Drukker, L., Papageorgiou, A.T., & Noble, J.A. (2020). Self-Supervised Representation Learning for Ultrasound Video. 2020 IEEE 17th International Symposium on Biomedical Imaging (ISBI), 1847-1850.
- [4] Noroozi, M., & Favaro, P. (2016). Unsupervised Learning of Visual Representations by Solving Jigsaw Puzzles. *ECCV*.
- [5] Misra, I., Zitnick, C.L., & Hebert, M. (2016). Shuffle and Learn: Unsupervised Learning Using Temporal Order Verification. *ECCV*.
- [6] Fernando, B., Bilen, H., Gavves, E., & Gould, S. (2017). Self-Supervised Video Representation Learning with Odd-One-Out Networks. 2017 IEEE Conference on Computer Vision and Pattern Recognition (CVPR), 5729-5738.
- [7] Gidaris, S., Singh, P., & Komodakis, N. (2018). Unsupervised Representation Learning by Predicting Image Rotations. *ArXiv*, abs/1803.07728.
- [8] Misra, I., & Maaten, L.V. (2019). Self-Supervised Learning of Pretext-Invariant Representations. *ArXiv*, abs/1912.01991.
- [9] Yamaguchi, S., Kanai, S., Shioda, T., & Takeda, S. (2019). Multiple Pretext-Task for Self-Supervised Learning via Mixing Multiple Image Transformations. *ArXiv*, abs/1912.11603.
- [10] Keshav, V., & Delattre, F. (2020). Self-supervised visual feature learning with curriculum. *ArXiv*, abs/2001.05634.
- [11] Newell, A., & Deng, J. (2020). How Useful is Self-Supervised Pretraining for Visual Tasks? *ArXiv*, abs/2003.14323.
- [12] Knights, J., Vanderkop, A., Ward, D., Mackenzie-Ross, O., & Moghadam, P. (2020). Temporally Coherent Embeddings for Self-Supervised Video Representation Learning. *ArXiv*, abs/2004.02753.
- [13] Kolesnikov, A., Zhai, X., & Beyer, L. (2019). Revisiting Self-Supervised Visual Representation Learning. 2019 IEEE/CVF Conference on Computer Vision and Pattern Recognition (CVPR), 1920-1929.
- [14] Jing, L., & Tian, Y. (2020). Self-supervised Visual Feature Learning with Deep Neural Networks: A Survey. *IEEE transactions on pattern analysis and machine intelligence*.
- [15] Dosovitskiy, A., Fischer, P., Springenberg, J.T., Riedmiller, M.A., & Brox, T. (2016). Discriminative Unsupervised Feature Learning with Exemplar Convolutional Neural Networks. *IEEE Transactions on Pattern Analysis and Machine Intelligence*, 38, 1734-1747.
- [16] Srivastava, N. (2015). Unsupervised Learning of Visual Representations using Videos.
- [17] El-Nouby, A., Zhai, S., Taylor, G.W., & Susskind, J.M. (2019). Skip-Clip: Self-Supervised Spatiotemporal Representation Learning by Future Clip Order Ranking. *ArXiv*, abs/1910.12770.
- [18] Larsson, G. (2017). Discovery of Visual Semantics by Unsupervised and Self-Supervised Representation Learning. *ArXiv*, abs/1708.05812.
- [19] Xu, D., Xiao, J., Zhao, Z., Shao, J.B., Xie, D., & Zhuang, Y. (2019). Self-Supervised Spatiotemporal Learning via Video Clip Order Prediction. 2019 IEEE/CVF Conference on Computer Vision and Pattern Recognition (CVPR), 10326-10335.
- [20] Jing, L., Yang, X., Liu, J., & Tian, Y. (2018). Self-Supervised Spatiotemporal Feature Learning via Video Rotation Prediction. *arXiv: Computer Vision and Pattern Recognition*.
- [21] Jing, L., & Tian, Y. (2018). Self-supervised Spatiotemporal Feature Learning by Video Geometric Transformations. *ArXiv*, abs/1811.11387.
- [22] Pathak, D., Krhenbhl, P., Donahue, J., Darrell, T., & Efros, A.A. (2016). Context Encoders: Feature Learning by Inpainting. 2016 IEEE Conference on Computer Vision and Pattern Recognition (CVPR), 2536-2544.
- [23] Zhang, R., Isola, P., & Efros, A.A. (2016). Colorful Image Colorization. *ArXiv*, abs/1603.08511.
- [24] Buckchash, H., & Raman, B. (2019). Sustained Self-Supervised Pre-training for Temporal Order Verification. *PREMI*.
- [25] Doersch, C., Gupta, A., & Efros, A.A. (2015). Unsupervised Visual Representation Learning by Context Prediction. 2015 IEEE International Conference on Computer Vision (ICCV), 1422-1430.
- [26] Lin, M., Chen, Q., & Yan, S. (2014). Network In Network. *CoRR*, abs/1312.4400.
- [27] Masko, D., & Hensman, P. (2015). The Impact of Imbalanced Training Data for Convolutional Neural Networks.
- [28] Zhuang, F., Qi, Z., Duan, K., Xi, D., Zhu, Y., Zhu, H., Xiong, H., & He, Q. (2019). A Comprehensive Survey on Transfer Learning. *ArXiv*, abs/1911.02685.
- [29] Engelen, J.E., & Hoos, H.H. (2019). A survey on semi-supervised learning. *Machine Learning*, 109, 373 - 440.
- [30] Mey, A., & Loog, M. (2019). Improvability Through Semi-Supervised Learning: A Survey of Theoretical Results. *ArXiv*, abs/1908.09574.
- [31] Rony, J., Belharbi, S., Dolz, J., Ayed, I.B., McCaffrey, L., & Granger, E. (2019). Deep weakly-supervised learning methods for classification and localization in histology images: a survey. *ArXiv*, abs/1909.03354.